UNIVERSITÀ DEGLI STUDI DI PARMA

MEAN FIELD TRANSPORT OF ULTRACOLD ATOMS THROUGH ENGINEERED POTENTIALS

Mailoud Sekkouri Samy

Supervisor
Prof. Wimberger SANDRO

Thursday 21st April, 2016

Contents

Chapter 1

Introduction

The possibility of realizing systems at extremely low temperatures provided new tools to investigate the quantum nature of matter. One of this tools regards the quantum transport of ultracold atoms, which only recently has been investigated in various setups with ultracold fermions and bosons [1, 2, 3, 4].

Quantum transport is an essential topic in solid state physics and electronic applications, for which the tunneling is one of the most important processes. However, due to complications such as impurities, lattice vibrations, and multi particle interactions clean observations of these effects have been difficult in crystals. The introduction of ultracold atoms in optical lattices gave the opportunity to work at quasi-zero temperature and to have experimental control on most of the system parameters as the lattice depth, the lattice periodicity or the strength of the atom-atom interactions. This makes atomic systems attractive as model systems for crystal lattices. The conceptual simplicity in such systems allows an efficient investigation and understanding of the microscopic transport. Optical lattices are nowadays easy to realize in the laboratory, and their parameters can be perfectly controlled both statically and dynamically. By superimposing laser beams from different directions and with slightly different wave-lengths, it is possible to generate many different three-dimensional lattice geometries [8].

In this thesis, our results for different engineered potentials are presented. This systems are realized with ultracold atoms forming a Bose–

Einstein condensate in an optical lattice subjected to a static tilting force [8]. The tilt is experimentally implemented by accelerating the optical lattice [6, 10]. We investigate the transport of Bose-Einstein condensates in different chosen parameter of the potential. To do this we start preparing the initial state as the ground state of an harmonic oscillator and than open the trap in one direction, so that the wave propagate only in that direction. We investigate in detail how the particle current in such a setup depends on the interactions which we treat in mean-field approximation following the Gross–Pitaevskii equation [11].

Chapter 2:

In this chapter we provide the theoretic for our studies. We start with a short review on the bosonic system of ultracold atoms and the formation of Bose–Einstein condensate in section 2.1. In the first part of this section, the non-interacting dilute Bose-gas and in the second part, the interacting Bose–gas in the regime of weak atom-atom interactions is shortly reviewed. The dynamics of Bose–Einstein condensates in such a regime is very well described in a mean-field regime based on the so-called Gross–Pitaevskii equation. Section 2.2 presents this non-linear Hamiltonian to describe the dynamics of condensate atoms, that are trapped in a three-dimensional harmonic oscillator potential. Bose–Einstein condensates in optical lattices are used to simulate solid state systems. Section 2.3 presents how the optical lattices can be created theoretically and experimentally through the interaction between atoms and light. Later in section 2.3, it is described that more complex and non-periodic optical lattices can be generated easily by superimposing more laser beams with arbitrary frequency difference.

Due to the Stark force it is possible to tilt the optical lattices. Particles in periodic potential and in the presence of the external field perform oscillatory movements. The so-called Bloch oscillation phenomenon is described in section 2.4. The problem of finding the eigenstates of the periodic system under the influence of an external field, the so-called Wannier–Stark problem is introduced in section 2.5.

Section 2.6 shows simply transformations in the system of natural units

which makes the numerical calculus without carrying big constant value.

Chapter 3:

In order to describe the dynamics of our systems, we need to integrate the Gross–Pitaevskii equation. Our numerical integration method is presented in chapter 3. Starting from the integration scheme in one dimension and its discretization. Then we present the predictor-corrector method which helps to get a better approximation when the Hamiltonian present a non-linear term. In order to prepare the initial state, we use an imaginary time method to integrate the Hamiltonian. We discuss these methods for a one-dimensional system and we introduce a method to ignore the non limitless of the grid: the absorption method.

Chapter 4: Finally we show our results, yet to be tested experimentally, we propose this contribution a relatively simple method to prepare the initial state, namely within a steep harmonic trap. Transport occurs when the trap is opened in one direction. We investigate in detail how the particle current in such a setup depends on the interactions which we treat in mean-field approximation following the Gross–Pitaevskii equation. We present how the interaction acts on the evolution of a wave packet in free half space, and in two optical tilted lattice with different parameters.

Chapter 5: We conclude showing fewer applications and a method to approach the problem of the more general three dimensional case, for cylindrical systems, can be reduced to a two dimensional problem in principle, which otherwise it requires a lot of time in calculations. We introduce here the problems we encountered and a partial solution to them.

Chapter 2

Ultracold atoms

2.1 Bose-Einstein condensation

At the beginning of the 20th century, following the work of Bose on the statistics of photons [16], Einstein considered a gas of non-interacting massive particles, and concluded that, below a critical temperature, of about one hundred nano Kelvin, a finite fraction of the total number of particles would occupy the lowest energy single-particle state [17]. Such a system undergoes a phase transition and forms a Bose-Einstein condensate, where a macroscopic number of particles occupy the fundamental energy state.

According to the theory of an ideal quantum gas of particles with mass M conform to Bose-Einstein statistics, at temperature T, a phase transition occurs when the De Broglie wavelength of characteristic thermal motions: $\lambda_B = (2\pi\hbar/Mk_BT)^{1/2}$, becomes comparable to the mean inter-particle separation: $r = n^{-1/3}$. Where k_B is the Boltzmann constant and n is the atom number density. The particle density at the centre of a Bose-Einstein condensate is typically $\sim 10^{13} - 10^{15} cm^{-3}$ [11]. In order to observe quantum phenomena at such low density, the temperature of the system must be of the order of $10^{-5}K$ or less. Laser cooling methods are used to cool down alkali metal atoms, but since these techniques alone cannot produce sufficiently high densities and low temperatures for condensation, it is followed by an evaporative cooling stage. During the latter stage, more energetic atoms are removed from the trap, and as result the remaining atoms are cooled further.

A microscopic population of atoms is achieved at such low temperature [8].

2.1.1 Non-interacting dilute Bose-gas

Every realistic Bose gas shows some level of particle-particle interaction. Therefore, the system of an ideal gas consisting of non-interacting Bosons is a fictitious system. Nevertheless, this model provides the simplest example for the realization of Bose-Einstein condensation. At zero temperature, a non-interacting Bose gas is fully condensed and all N particles are described by identical single particle wave function [11]. The many body ground state wave function in then given by the product of N identical ground state functions.

$$\Psi(\mathbf{r}_1, \mathbf{r}_2, ..., \mathbf{r}_N) = \prod_{i=1}^{N} \psi(\mathbf{r}_i) \tag{2.1}$$

This condensate wave function is a normalized macroscopic wave function. For a non-interacting Bose gas and an inhomogeneous system, this state is simply the single particle ground state of the confining potential.

2.1.2 Interacting Bose gas in the mean-field limit

When weak interactions between particles are included in the problem, the ground state many body wave function is still, to a very good approximation, a product of N single particle wave functions. These functions are now obtained from the solution of a non-linear Schrödinger equation [8], which is known as Gross–Pitaevskii equation and describes the dynamics of weakly interacting bosons. The condensate typically consists of a few thousands to millions of atoms which are confined by a trapping potential. The macroscopic behaviour of the Bose-Einstein condensate is affected by the internal interactions between the atoms, and by the shape of the external trapping potential. The atom-atom interaction in a cold dilute gas of bosons is dominated by elastic binary collisions and can be treated in the framework of scattering theory. At very low temperatures, the thermal de Broglie wavelength λ_B is much larger than the mean inter-particle separation, thus

only s-wave collision are important. For such a dilute gas the interactions can be modeled by a Dirac delta potential whose strength is proportional to the s-wave scattering length a_s. The inter-atomic potential can be replaced by an effective contact interaction:

$$V = \frac{4\pi\hbar^2 a_s}{M}\delta(\mathbf{r}) \equiv g\delta(\mathbf{r}) \tag{2.2}$$

where $\mathbf{r}$ is the relative coordinate between two atoms, M is the mass of the single atom, a_s is the s-wave scattering length and $g \equiv 4\pi\hbar^2 a_s/M$ is the coupling constant [11]. The strength of the two-body interaction ($\sim a_s$) in the ultracold atomic gas can be tuned by means of Feshbach resonances [18]. It is possible to create attractive interactions for negative a_s, repulsive interactions for positive a_s, or even non-interacting gases.

2.2 Gross–Pitaevskii Equation

For a dilute gas, the dynamics of a Bose-Einstein condensate can be described by the mean-field approximation. The diluteness of the gas is characterized by the ratio of scattering length a_s and the inter-particle spacing. This ratio can be expressed as a gas parameter na_s^3 and is typically less than 10^3. In this limit, due to the mean field of all other atoms in the condensate, each atom feels an additional potential. Therefore, the interaction potential to the local atomic density $|\psi(\mathbf{r},t)|^2$. The dynamic properties of a Bose-Einstein condensate at temperature $T < T_c$ are usually well modeled by a general non-linear Schrödinger equation for the macroscopic function, where the Hamiltonian reads:

$$H = \frac{\mathbf{p}^2}{2m} + V_{ext}(\mathbf{r}) + V_{int}(\mathbf{r},t) \tag{2.3}$$

This Hamiltonian contains the trap potential $V_{ext}(\mathbf{r})$, typically an harmonic oscillator potential, as well as the coupling interactions in the form of the non-linear term.

$$V_{int}(\mathbf{r},t) = g_{3D}N|\psi(\mathbf{r},t)|^2 \tag{2.4}$$

Where the coupling constant g_{3D} is the same as in Eq. (2.2), and N is the number of atoms in the condensate. the wave function is then normalized to 1. We restrict here to a system which is confined in an harmonic trap characterized by a frequency $\omega_\perp$ in the two transverse directions with radial symmetry. This system can be approximated to a quasi one-dimensional situation. This regime is obtained if the traverse confinement length $l_\perp \equiv \sqrt{\frac{\hbar}{M\omega_\perp}}$ is on the order of $\xi_h = \frac{1}{\sqrt{8\pi n a_s}}$ [11] where n is the mean particle density. In this regime we have to change the coupling constant in order to keep in consideration the others dimensions:

$$g_{1D} = 2\hbar\omega_\perp a_s \tag{2.5}$$

2.3 Optical Lattice

2.3.1 Connection to solid state physics

Following the classical experiments which showed the mechanical action of light on neutral atoms [19], proving the theoretical prediction of Maxwell that electromagnetic waves carry momentum, the development of the lasers made it possible to realize resonant light forces on neutral particles. Only in the 1970s the first scattering measurements were done using both travelling and standing waves [20]. In 1998 Anderson and Kasevich loaded a Bose-Einstein condensate in a standing light wave [7] which was the beginning point to study its dynamics in periodic potentials [8]. Optical lattices are periodic potentials created by light-atom interactions. When an atom interacts with an electromagnetic field, its internal states depends on the light intensity. Therefore, a spatially dependent intensity induces a spatially dependent potential energy [21]. The system of a particle in a periodic optical lattice is the textbook model of an electron in a crystal lattice. Optical lattices have several advantages with respect to solid state system. The optical system can be made free from defects, resulting in a larger mean free path of particles. Defects prevented for example the observation of the theoretically predicted coherent phenomenon such as Bloch

Oscillations. The lattice depth and geometry can be easily controlled by optical means. Using multiple-beam, interference makes it possible to realize two-dimensional and three-dimensional lattices, super-lattices, ratchets and more complex structures. In optical system the relaxation time can be made much larger than the coherent time scale. In addition, the possibility to dynamically control the interaction potential in real time during the experiment allowed recent experiments to observe many of the coherent effects, such as Bloch oscillations on the Wannier-Stark ladders, which are hardly accessible in solid state systems [5, 8, 22, 23, 24].

2.3.2 Interaction of atoms and light

Neutral atoms interact with a light field in both a dissipative and a conservative way. The conservative interaction comes from the interaction of the light field with the light induced dipole moment of the atom. It causes a shift in the potential energy, the so-called Stark shift. The dissipation arises due to the absorption of photons followed by spontaneous emissions. It results in a dissipative force on the atoms caused by the momentum transfer of the absorbed and spontaneously emitted photons. This light force is widely used for laser cooling and magneto optical traps [25]. For a large detuning of the light from atomic resonances, spontaneous emission processes can be neglected and the energy shift can be used to create a conservative trapping potential for neutral atoms [26]. Periodic optical potentials are created by superimposing two laser beams with the same frequency ω_L. The resulting electric field is of the form

$$E(\mathbf{r},t) = \frac{1}{2}E_0(e^{i(\mathbf{k_1}\cdot\mathbf{r}+\omega_L t)} + e^{i(\mathbf{k_2}\cdot\mathbf{r}-\omega_L t)}) + c.c. \tag{2.6}$$

where E_0 is the amplitude, $k_i = 2\pi/\lambda_i$ is the wave vector of the laser wavelength. The atom-field interaction energy is:

$$H_{int} = -\mathbf{d}\cdot\mathbf{E}(\mathbf{r},t) \tag{2.7}$$

Using two laser beams related by $k_1 = -k_2 = k_L$ leads to the effective interaction

$$V_{eff} = \frac{V_0}{2}\cos(2\mathbf{k_L}\cdot\mathbf{r}) \tag{2.8}$$

The amplitude of the periodic potential V_0 can be expressed in terms of the Rabi frequency Ω_R which can be rewritten in therms of the laser intensity I. This way the amplitude of the periodic potential can be expressed in terms of measurable quantities [6, 8]

$$V_0 = \frac{\hbar\Omega_R^2}{\Delta_L} = \zeta\hbar\frac{I}{I_s}\frac{\Gamma_s^2}{\Delta_L} \tag{2.9}$$

where $\Delta_L = \omega_L - \omega_0$ is the average detuning from resonance, I_s is the saturation intensity, ζ is a correction which depend on the level structure of the atom and Γ_s is the photon scattering rate [27]. Therefore, considering two counter-propagating laser beams along the x-axis, the resulting one-dimensional periodic potential can be written as $V = V_0\sin^2(k_l x)$.

2.3.3 Tilted optical lattice

Ultracold atoms in optical lattices can model the solid-state systems of electrons in a crystal in the presence of applied fields. The force induced by an external field is necessary to observe phenomena like Bloch oscillations and Wannier-Stark ladders. Such a force can be easily implemented in optical lattices, i.e. by an inertial force by accelerating the optical lattice [6].

$$H = \frac{p^2}{2M} + V_0\sin^2(k_L x) + Fx \tag{2.10}$$

This Hamiltonian presents the so-called Wannier-Stark system. The last term in the Hamiltonian mimics the role of the interaction potential $V_C = eEx$ between the electric field E and the electron of charge e in the crystals.

2.4 Bloch oscillations

In solid-state physics, the temporal dynamics of an electron facing an electric field is a fundamental quantum-mechanical problem. Felix Bloch

predicted the dynamical behaviour of electrons in a solid, subject to a uniform, static electric field [28]. It was expanded later by Zener, showing that electrons accelerated by an electric field in a periodic potential, under the right conditions, could oscillate [29]. The frequency of oscillations in given by $\omega_B = Fd_L/\hbar$, where $F = eE$ is the force and d_L is the lattice constant. This phenomenon is known as Bloch oscillations. Bloch oscillations have never been observed in natural crystals because the scattering time of the electrons at lattice defects is much shorter than the Bloch period. In fact only in 1992 the Bloch oscillations were detected using semiconductor superlattices [5, 22].

For a particle in a periodic potential $V(x) = V(x+d_L)$ in the presence of a force F, the Schrödinger equation can be written

$$i\hbar\frac{\partial}{\partial t}\psi(x,t) = \left(-\frac{\hbar^2}{2M}\frac{d^2}{dx^2} + V(x) + Fx\right)\psi(x,t) \tag{2.11}$$

it is assumed that the wave function has the following form

$$\psi(x,t) = \sum_{n,k} c_{n,k}(t)\psi_{n,k}e^{-iE_nt/\hbar} \tag{2.12}$$

and the time variation of the amplitude of the coefficients can be found as [28]

$$\frac{d}{dt}|c_{n,k}(t)|^2 = -\frac{F}{\hbar}\frac{\partial}{\partial k}|c_{n,k}(0)|^2 \tag{2.13}$$

A particle confined to a single energy band will move in the opposite direction of the field until being reflected by the lattice, and then it moves in the opposite direction until is stopped by the force, where it starts the same motion over again [29]. This periodic oscillation is characterized by the period

$$T_B = \frac{2\pi\hbar}{Fd_L} \tag{2.14}$$

Bloch oscillations in the time domain are related to the existence of a Wannier-Stark ladder in the frequency domain [31].

2.5 Wannier-Stark ladders

The dynamics of a particle in a one-dimensional periodic lattice potential $V(x) = V(x + d_L)$ under the influence of a force is described by the so-called Wannier–Stark Hamiltonian

$$H = \frac{p^2}{2M} + V_0 \sin^2(k_L x) + Fx \tag{2.15}$$

The problem of describing the spectrum of this system created a long standing discussion about its properties [30, 31, 32, 33, 34, 35]. This discussions were initiated due to a counter intuitive prediction and by the difficulty to verify the predictions experimentally. The application of a force destroys the translational invariance of the periodic potential and causes a gradual localization of the initially delocalized Bloch states which is called Stark localization [31]. The Wannier functions are in essence a Fourier transform of the Bloch states. Applying a force, the continuous density of states is transformed into a series of equally spaced - in energy and real space - ladder states with energies forming the Wannier–Stark ladder:

$$E_{n,m} = E_n + mFd_L, \quad m = 0, \pm 1, \pm 2... \tag{2.16}$$

where $E_{n,m}$ are the energy levels, E_n is the mean energy of the band, and mFd_L are the ladder spacing intervals with m being the site index and n the band index. This implies that if there exists an eigenstate $\psi_n(x)$ with energy En, then the set of states corresponding to wave functions $\psi_{n,m}(x) = \psi_n(x - md_L)$ are eigenstates of the Hamiltonian with energies $E_{n,m}$. The ladder spacing is related to the Bloch oscillation period T_B and leads to what is called Stark ladders.

2.6 External potential

To study the transport of a Bose-Einstein condensate in mean field approximation with a numerical approach, we prepare the wave function in the ground state of an harmonic trap. Transport occurs when the trap is

opened one direction. We investigate in detail how the particle current depends on the structure of the potential first without internal interaction and then switching it on following the Gross-Pitaevskii equation. Our potential can be written:

$$V_{ext}(x) = \begin{cases} \frac{1}{2}m\omega^2(x-x_0)^2 & t<0 \\ \theta(x_0-x)\frac{1}{2}m\omega^2(x-x_0)^2 - \theta(x-x_0)[Fx+\sin^2(K(x-x_0))] & t>0 \end{cases} \tag{2.17}$$

From now on we will see the transformations of the Hamiltonian only for $t>0$, because the case $t<0$ is included in it. The extended one dimensional Hamiltonian is then:

$$\begin{aligned} H(x,p) = \frac{p^2}{2m} + g|\psi(x,t)|^2 + \\ + \theta(x_0-x)\frac{1}{2}m\omega^2(x-x_0)^2 + \\ - \theta(x-x_0)[Fx+A\sin^2(K(+x-x_0))] \end{aligned} \tag{2.18}$$

2.6.1 Natural units

To simplify the problem, we rescale Eq. (2.18) by introducing dimensionless variables,

$$\begin{cases} p \equiv (\hbar\omega m)^{\frac{1}{2}}\tilde{p} \\ x \equiv (\frac{\hbar}{\omega m})^{\frac{1}{2}}\tilde{x} \end{cases} \tag{2.19}$$

where ω is the harmonic trap frequency at $t=0$. Imposing that the norm remains the same $\int|\psi|^2dx = \int|\tilde{\psi}|^2d\tilde{x} = 1$ we obtain the transformation for the wave function:

$$|\psi|^2 = \frac{d\tilde{x}}{dx}|\tilde{\psi}|^2 = \left(\frac{\omega m}{\hbar}\right)^{\frac{1}{2}}|\tilde{\psi}|^2 \tag{2.20}$$

Replacing this in the Hamiltonian we have:

$$\begin{aligned}\tilde{H}(\tilde{x},\tilde{p}) \equiv \frac{1}{2}\tilde{p}^2 + \tilde{g}|\tilde{\psi}(\tilde{x},\tilde{t})|^2 + \\ + \frac{1}{2}\theta(\tilde{x_0}-\tilde{x})(\tilde{x}-\tilde{x_0})^2 + \\ - \theta(\tilde{x}-\tilde{x_0})[\tilde{F}\tilde{x} + \tilde{A}\sin^2(\tilde{K}(\tilde{x}-\tilde{x_0}))]\end{aligned} \tag{2.21}$$

where the new constants become $\tilde{g} \equiv g(m/\hbar^3\omega)^{1/2}$, $\tilde{F} \equiv F/(\hbar\omega^3 m)^{1/2}$, $\tilde{A} \equiv A/\hbar\omega$, $\tilde{K} \equiv K(\hbar/\omega m)^{1/2}$, $\tilde{H} \equiv H/\hbar\omega$.

The transformation of time we get from the Schrödinger equation:

$$i\hbar\frac{\partial}{\partial t}\psi(x,t) = H(x)\psi(x,t) = \hbar\omega\tilde{H}(x)\psi(x,t) \tag{2.22}$$

in our units the system can be rewritten as:

$$i\frac{\partial}{\partial \tilde{t}}\tilde{\psi}(\tilde{x},\tilde{t}) = \tilde{H}(\tilde{x})\tilde{\psi}(\tilde{x},\tilde{t}) \tag{2.23}$$

where $\tilde{t} \equiv \omega t$ is time in our units. In the remaining part of the thesis we use the dimensionless units introduced above. We leave away the tildes for simplicity in what follows.

Chapter 3

Numerical Methods

In order to integrate the Gross-Pitaevskii equation, we used a numerical approach. In this chapter, an implicit integration procedure is introduced, based on numerical evaluation of the time evolution operator. This is applied to the representation of the wave function in a spatial grid basis. Since the Bose-Einstein condensate can be prepared with certain symmetries due to the trap, different coordinates representations can be considered. This can reduce the three dimensional Gross-Pitaevskii equation into a quasi one dimensional one.

3.1 Integration scheme in one-dimension

In this section, an implicit method to solve the partial differential equation given by a one dimensional Gross-Pitaevskii equation is presented. The time evolution of the wave function $\psi(x,t)$ is described as

$$\begin{aligned} i\frac{\partial}{\partial t}\psi(x,t) &= H(x)\psi(x,t) \\ H(x,t) &= -\frac{1}{2}\frac{\partial^2}{\partial x^2} + V_{ext}(x) + g_{1D}|\psi(x,t)|^2 \end{aligned} \tag{3.1}$$

where $V_{ext}(x)$ is the external potential, $g_{1D} \equiv 2\hbar\omega_\perp a_s N$ is the one dimensional coupling constant for the weak atom-atom interactions of the condensate atoms. The Gross-Pitaevskii equation represents a non-linear

time dependent Schrödinger equation.

The solution to this time dependent equation in the Schrödinger representation is given by

$$\psi(x,t) = U(t,t_0)\psi(x,t_0) \tag{3.2}$$

where the time evolution operator is defined as

$$\begin{aligned} U(t,t_0) &= \mathbf{T}\left(-i\int_{t_0}^{t} dt' H(x,t') \right) \\ &= 1 - i\int_{t_0}^{t} dt_1 H(x,t_1) + (i)^2 \int_{t_0}^{t} dt_1 \int_{t_0}^{t_1} dt_2 H(x,t_1)H(x,t_2) + ... \end{aligned} \tag{3.3}$$

The non-linear term $g_{1D}|\psi(x,t)|^2$ is considered as a self consistent time dependent effective potential. For small time difference Δt, according to the mean-value theorem the above integral can be approximated as

$$U(t+\Delta t,t) = 1 - iH(x,t)\Delta t + (i)^2 H^2(x,t)\Delta t^2 + ... \tag{3.4}$$

Knowing the state $\psi(x,t)$ at time t, the wave function $\psi(x,t+\Delta t)$ at time $t+\Delta t$ can now be calculated by Eq. (3.2). Taking into account only the terms of the order $O(\Delta t)$, a simple solution reads

$$\psi(x,t+\Delta t) = \left[1 - iH(x,t)\Delta t \right] \psi(x,t) \tag{3.5}$$

But since the operator $[1 - iH(x,t)\Delta t]$ is not unitary, this explicit integration method is numerically unstable [44], and moreover, it does not conserve the normalization of the wave function. To circumvent these disadvantages, the Cayley's theorem can be used which results in the following presentation of time evolution operator [45]

$$\psi(x,t+\Delta t) = \frac{1 - \frac{i}{2}H(x,t)\Delta t}{1 + \frac{i}{2}H(x,t)\Delta t}\psi(x,t) \tag{3.6}$$

This approximation has error on the order of $O(\Delta t^3)$. This error can be determined by comparing the power series of the time evolution operator given in Eq. (3.6) with the power series of $exp(-iH\Delta t)$. Taking the first four terms in the power series expansion of this time evolution operator reads

$$e^{-iH\Delta t} = 1 - iH\Delta t - \frac{(H\Delta t)^2}{2} + i\frac{(H\Delta t)^3}{6} + ... \tag{3.7}$$

while the expansion for the approximation gives

$$\frac{1 - \frac{i}{2}H(x,t)\Delta t}{1 + \frac{i}{2}H(x,t)\Delta t} = 1 - iH\Delta t - \frac{(H\Delta t)^2}{2} + i\frac{(H\Delta t)^3}{4} + ... \tag{3.8}$$

These two expansions differ beginning only in the third term, and the error will be of the third order. With this unitary time-evolution operator, the norm of the wave function is also conserved. Eq. (3.6) results in the following integration algorithm:

$$\left[1 + \frac{i}{2}H(x,t)\Delta t\right]\psi(x,t+\Delta t) = \left[1 - \frac{i}{2}H(x,t)\Delta t\right]\psi(x,t) \tag{3.9}$$

In numerical analysis, this type of solution is called an implicit scheme or a Crank–Nicholson scheme [44]. In the numerical simulation of the time evolution over a total time period $\Delta T = t_f - t_i$ (with $t_f > t_i$), we divide ΔT into N_t equal time intervals $\Delta t = \Delta T / N_t$. The aim is to calculate numerically the wave function of the discrete times $t_n = n\Delta t$, by means of the implicit scheme given in Eq. (3.9). To solve this equation numerically, one must discretize Eq. (3.1). In the following, the discretization process is presented.

3.1.1 Expansion over a grid

To solve the Gross-Pitaevskii equation given in Eq. (3.1), the wave function is expanded over a discrete basis. The continuous variable x is represented as a discrete variable $x_j = x_0 + j\Delta x$, where Δx is the mesh size, x_0

the starting value, and j is an integer which runs from 1 to N_x. Time is also represented as a discrete variable as $t_n = t_0 + n\Delta t$, where Δt is the time step, t_0 the initial time and n is an integer. Both x_0 and t_0 can be set to zero for simplicity. We can define the following basis states

$$\chi_j \equiv \begin{cases} 1, & x_j - \frac{1}{2}\Delta x \leq x \geq x_j - \frac{1}{2}\Delta x \\ 0, & otherwise \end{cases} \tag{3.10}$$

The wave function is therefore expanded over this discrete space as $\psi(x_j,t_n) = \sum_{j=1}^{N_x} \psi_j^n \chi_j$, where the expansion coefficient, at time t_n, is $\psi_j \equiv \psi_j^n$

The form of the wave function is a column vector, with each component taken at the mesh point, such that for any time t, the wave function can be rewritten as

$$\psi^n(x) = \begin{pmatrix} \psi(\Delta x) \\ \psi(2\Delta x) \\ \psi(3\Delta x) \\ . \\ . \\ . \\ \psi(N_x\Delta x) \end{pmatrix} \tag{3.11}$$

In our numerical calculation N_x is typically on the order $\sim 2^{12}$. The potential term in the Hamiltonian is a function of x, therefore, the discrete representation of $V(x)$, at time t_n, is

$$V^n(x) = \begin{pmatrix} V(\Delta x) \\ V(2\Delta x) \\ V(3\Delta x) \\ . \\ . \\ . \\ V(N_x\Delta x) \end{pmatrix} \tag{3.12}$$

The interaction term consists of the time-dependent wave function and can also be generated at each time step as $g_{1D}|\psi(x,n\Delta t)|^2 \equiv g_{1D}|\psi_j^n|^2$. The discretization of the kinetic energy operator is more involved. A proper discrete representation for the second spatial derivative can be found using a finite difference method. The Crank–Nicolson method is a finite difference method which is based on central difference in space, and the trapezoidal rule in time, giving second-order convergence in time. This method provides a discrete representation for the kinetic term

$$-\frac{1}{2}\frac{\partial^2\psi_j^n}{\partial x^2} = -\frac{1}{2}\frac{\psi_{j+1}^n + \psi_{j-1}^n - 2\psi_j^n}{\Delta x^2} \tag{3.13}$$

where ψ_j^n is in fact $\psi(j\Delta x, n\Delta t)$. Therefore the Hamiltonian operating on $\psi(x,t)$ has the following discrete form

$$H\psi_j^n = -\frac{1}{2\Delta x^2}[\psi_{j+1}^n + \psi_{j-1}^n - 2\psi_j^n] + V_j\psi_j^n + g_{1D}|\psi_j^n|^2\psi_j^n \tag{3.14}$$

The mesh runs from $j = 1,...,N_x$, therefore, for solving this equation, values for $\psi(0)$ and $\psi((N_x+1)\Delta x)$ are needed, which are outside the mesh system. These values are simply set to zero. Of course, this is like assuming the potential is suddenly infinite outside the mesh system. Practically, the spatial system should be constructed sufficiently large so that, over the time scales of interest, the wave functions do not reflect from these "hard walls". Since we are studying the transport of the condensate, it is in our interest to make the wave travel far enough, therefore we will introduce an absorption method of the wave function beyond a fixed position. As a result of the discretization, a single differential equation is thus replaced with a set of N_x coupled equations. The Hamiltonian has the form of an $N_x \times N_x$ matrix:

$$H = \begin{bmatrix} -2k+K & k & 0 & & . & . & .0 \\ k & -2k+K & k & 0 & & & : \\ 0 & ... & ... & ... & & & 0 \\ ... & ... & ... & ... & & & : \\ 0 & ... & 0 & ... & 0 & k & -2k+K \end{bmatrix} \tag{3.15}$$

where $k = -\frac{1}{2\Delta x^2}$ and $K = V_j + g_{1D}|\psi_j^n|^2$. As seen, the Hamiltonian H is a tridiagonal matrix, with non-zero term only on the main diagonal and the first upper and lower diagonals. To reduce the memory required for this calculation, only non-zero terms are stored. Using the discrete representation of the Hamiltonian the terms $[1 \pm iH\Delta t/2]\psi(x_j, t_n)$ in the discrete form reads

$$\psi_j^n \pm \frac{i\Delta t}{2}\left[\frac{1}{2\Delta x^2}[\psi_{j+1}^n + \psi_{j-1}^n - 2\psi_j^n] + V_j\psi_j^n + g_{1D}|\psi_j^n|^2\psi_j^n\right] \tag{3.16}$$

Using the matrix representation, one finds the following tridiagonal matrix for the operators $M_\pm \equiv 1 \pm iH\Delta t/2$

$$M_\pm = \begin{bmatrix} . & & & & & & & \\ & . & & & & & & \\ & & \mp\alpha & 1 \pm \beta_{j-1} & \mp\alpha & & & \\ & & & \mp\alpha & 1 \pm \beta_j & \mp\alpha & & \\ & & & & \mp\alpha & 1 \pm \beta_{j+1} & \mp\alpha & \\ & & & & & & . & \\ & & & & & & & . \end{bmatrix} \tag{3.17}$$

where

$$\begin{aligned} \alpha &\equiv \frac{i\Delta t}{4\Delta x^2} \\ \beta_j &\equiv \frac{i\Delta t}{2\Delta x^2} + \frac{i\Delta t}{2}(V_j + g_{1D}|\psi_j^n|^2) \end{aligned} \tag{3.18}$$

Therefore the numerical evaluation of the implicit integration scheme given in Eq. (3.9) is described by the following matrix equation

$$M_+\psi^{n+1} = M_-\psi^n \quad \Rightarrow \quad \psi^{n+1} = M_+^{-1}M_-\psi^n \tag{3.19}$$

The vectors ψ^n and ψ^{n+1} are wave functions at time t_n and t_{n+1}, respectively. The above equation has the form of $\mathbf{A}\cdot\vec{X} = \vec{b}$, where $\vec{b}$ is an $N_x \times 1$ column vector and equals $M_-\psi^n$, the matrix $\mathbf{A} = M_+$ and $\vec{X} = \psi^{n+1}$ is what

has to be found, through solving the above equation. In our numerical simulation, we solve this matrix equation using Gaussian elimination method for tridiagonal matrices [44]. This algorithm allows to calculate the inversion without actually storing the matrix, one only needs to store its non-zero elements as a vector.

3.1.2 Predictor-Corrector method

Due to the non-linear term $g_{1D}|\psi_j^n|^2$, the Hamiltonian is time dependent. Starting from $\psi(x,t)$, using the matrix representation of the integration scheme, one can calculate $\psi(x,t+\Delta t)$. Therefore, the wave function $\psi(x,t)$ at time t is used in the matrices M_+ and M_-. This assumes, however, the approximation that the effective potential $g_{1D}|\psi|^2$ induced by the non-linearity is not changing during the time interval Δt. In principle, the error caused by this approximation can be reduced by choosing an infinitesimally small time interval Δt for the numerical integration. Due to such a small time interval, it becomes necessary to have a larger number of matrix inversions which causes a growth of numerical costs. To deal with this problem, a two step Predictor–Corrector method [44] is used in our simulations, which allows to reduce the approximation error induced by the non-linearity, without being forced to use an infinitesimally small time interval Δt. The basic idea is to use the averaged value over the time interval for the wave function, instead of the wave function $\psi(x,t)$. Therefore, each integration step is really done two times to go from time t to time $t+\Delta t$. In the first time, $\psi(x,t)$ is used in the non-linear term, and a "predicted" wave function $\tilde{\psi}(x,t+\Delta t)$ is obtained, This is the so-called predictor step. In the second time, the integration step is repeated starting again from $\psi(x,t)$, but placing the averaged value $g_{1D}|\frac{1}{2}(\psi(x,t)+\tilde{\psi}(x,t+\Delta t))|$ in the non-linear term. In this way, in this so-called corrector-step, an already better approximate value for the non-linear term is used. This process is represented schematically here:

$$
\begin{aligned}
&\textit{Predictor step}: \\
&\qquad \psi(x,t) \xrightarrow{g_{1D}|(\psi(x,t)|^2} \tilde{\psi}(x,t+\Delta t) \\
&\textit{Corrector step}: \\
&\qquad \psi(x,t) \xrightarrow{g_{1D}|\frac{1}{2}(\psi(x,t)+\tilde{\psi}(x,t+\Delta t))|} \psi(x,t+\Delta t)
\end{aligned}
\tag{3.20}
$$

3.1.3 Ground state

The numerical method developed in this chapter, can be used not only to simulated the time evolution of a Bose-Einstein condensate, but also it allows calculating the ground-state wave function $\psi_0(x)$ of a condensate in an external potential. The ground state is the lowest energy state of a solution of the Schrödinger or the Gross-Pitaevskii equation. Here, we introduce a method which is known as the time-imaginary propagation [46], which allows the calculation of the ground state wave function. In this method the imaginary time are $t \to \tau = -it$ which leads to the transformation in the time interval $\Delta t \to \Delta\tau = -i\Delta t$. By these substitutions, the evolution become the following non linear diffusion equation

$$
\frac{\partial}{\partial\tau}\psi(x,\tau) = \left[-\frac{1}{2}\frac{\partial^2}{\partial x^2} + V_{ext}(x) + g_{1D}|\psi(x,\tau)|^2 \right] \psi(x,\tau) \tag{3.21}
$$

The process of finding the ground state of this equation is quite similar to the process of finding the wave function at time τ of the real time evolution explained previously. The implicit integration scheme given in Eq. (3.9) is also used for the imaginary propagation in the following modified form

$$
\left[1 + \frac{1}{2}H(x,\tau)\Delta\tau\right]\psi(x,\tau+\Delta\tau) = \left[1 - \frac{1}{2}H(x,\tau)\Delta\tau\right]\psi(x,\tau) \tag{3.22}
$$

Using the discrete forms of wave function and the Hamiltonian, one can arrive at the matrix representation

$$
\psi^{n+1} = \tilde{M}_+^{-1}\tilde{M}_-\,\psi^n \tag{3.23}
$$

with

$$\tilde{M}_{\pm} = \frac{1}{i}\begin{bmatrix} . & & & & & & \\ & . & & & & & \\ & & \mp\alpha & 1\pm\beta_{j-1} & \mp\alpha & & \\ & & & \mp\alpha & 1\pm\beta_j & \mp\alpha & \\ & & & & \mp\alpha & 1\pm\beta_{j+1} & \mp\alpha \\ & & & & & & . \\ & & & & & & . \end{bmatrix} \tag{3.24}$$

In order to determine the ground state wave function with the imaginary propagation, the iteration scheme used is

$$\begin{aligned} &Propagation: \\ &\qquad \psi^{n+1} = \tilde{M}_{+}^{-1}\tilde{M}_{-}\psi^{n} \\ &Renormalization: \\ &\qquad \psi^{n+1} \rightarrow \psi^{n+1} = \sqrt{N/\tilde{N}} \end{aligned} \tag{3.25}$$

where $N \equiv \int_{-\infty}^{\infty} |\psi_0(x)|^2$ which is equal to 1 in most case, and $\tilde{N} \equiv \int_{-\infty}^{\infty} |\psi(x, t_0 + \Delta t)|^2 \leq N$, until a given initial wave function $\psi^{n=0}$ has developed to a steady wave function. Numerically, this can be implemented, by computing the maximum norm difference $N_{max} \equiv max_j |\psi_j^{n+1} - \psi_j^n|$ for each integration step. Once N_{max}, over several propagation steps, become smaller than a predetermined limit δ, one can say that the stationary ground state in the desired precision has been achieved.

3.2 Absorption method on a grid

In the numerical simulation of wave propagation, by spatially discrete methods, the evolution itself of a wave packet presents some issues: for example it's impossible to create a grid indefinitely large with fixed step. Reflections from the boundaries of numerical grids have always presented a difficulty in applying discrete methods to simulate physical phenomena.

This problem is very important in the case the evolution of the wave packet reaches the edges of the grid. One solution could be adding a periodic boundary conditions, making the wave evolve in a closed circle ($1D$). This method could be inconvenient in our case, because it brakes the tridiagonal symmetry of the Hamiltonian causing a significant increase at the time of calculus (see section 3.1.1). Our solution of this problem, came from the idea that most of the observables, of our interest, depend on the value of the wave packet in a neighbourhood of positions. Therefore, there will be a point in the grid beyond that the value of the wave is not interesting. From this idea we introduced a method of absorption of the wave beyond a fixed position $x > x_A$. The importance of absorbing boundaries has been recognized in the past and consequently a number of methods have been proposed for constructing absorbing boundaries [47, 48, 49]. Lysmer and Kuhlemeyer [47] proposed a method based on viscous damping on the boundaries of the numerical mesh. A class of methods derived more recently is based on replacing the wave equation on the boundary grid points by a one way equation which allows energy to propagate in the outward direction only [48, 49].

There are different numerical methods of doing this, based on a simple modification of the wave or the wave equation so that the wave amplitude becomes attenuated at the grid boundary region. We will discuss only two of them in the following.

The first one consists in multiplying, at each time step, the wave in the absorption region $\psi(x > x_A)$ by a function which values are $0 \leq f(x) \leq 1$, as smooth as possible.

$$\psi(x) \to f(x)\psi(x), \quad x > x_A \tag{3.26}$$

for example one can use a sigmoid function as follow

$$f(x) \sim 1 - \frac{1}{1 + \exp(-L(x - x_C))} \tag{3.27}$$

The second method consists in adding to the Hamiltonian an imaginary smooth potential, that acts as an absorption trap.

$$H(x) \to H(x) - iV(x), \quad x > x_A \tag{3.28}$$

i.e. one can use an exponential for the imaginary potential as follow

$$V(x) \sim e^{L(x-x_A)^\alpha} - 1 \tag{3.29}$$

These kind of methods are highly dependent on the type of wave equation and the spatial discretization, therefore one must test them and find the optimal parameters. To test this methods one can compare wave function after the evolution in these situations $\psi(x)$ with the evolution of the wave function in a grid large enough in which the wave doesn't reaches the edges $\psi_{true}(x)$. This comparison can be expressed by the calculus of the variance

$$\sigma^2 = \frac{\int_0^{x_A} |\psi(x) - \psi_{true}(x)|^2 dx}{\int_0^{x_A} |\psi_{true}(x)|^2 dx} \tag{3.30}$$

The variance can be used to optimize the parameters of the absorption function and the imaginary potential. Another way to optimize the parameters is to calculate the Fourier transform of the wave function, and then minimize the reflections in the momentum space. In our case, we tested the two methods by studying the evolution of a free wave function initially prepared in the state of a Gaussian shifted in the momentum space, comparing it with the evolution of the same wave but in a grid big enough in which it doesn't reach the edges.

Optimizing the parameters in function of the kinetic energy of the incoming wave to minimize the variance, we obtained, for this particular case a significant better approximation for the second method as shown in Fig. 3.2. Thus for our results we decided to use the second method.

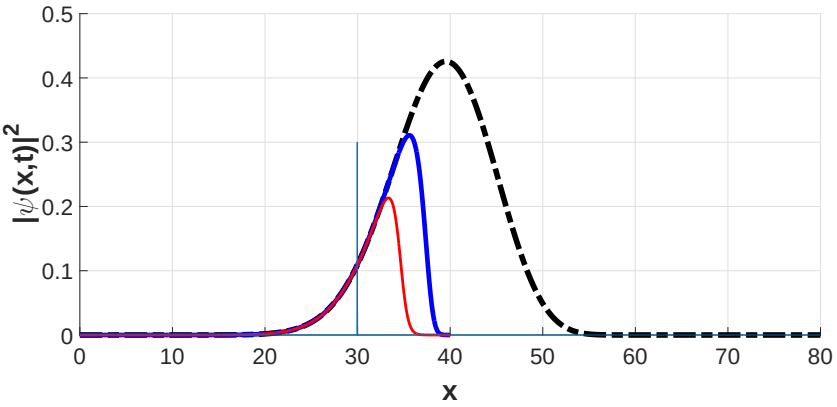

Figure 3.1: Comparison of the wave functions evolved using the first method of absorption (red continuous line), the second one (blue continuous line) discussed above and the true evolved wave function (black dotted line) evolved in a grid large enough in which the wave doesn't reach the edges. The absorption point has been placed in $x = x_a = 30$, it is indicated by the vertical line.

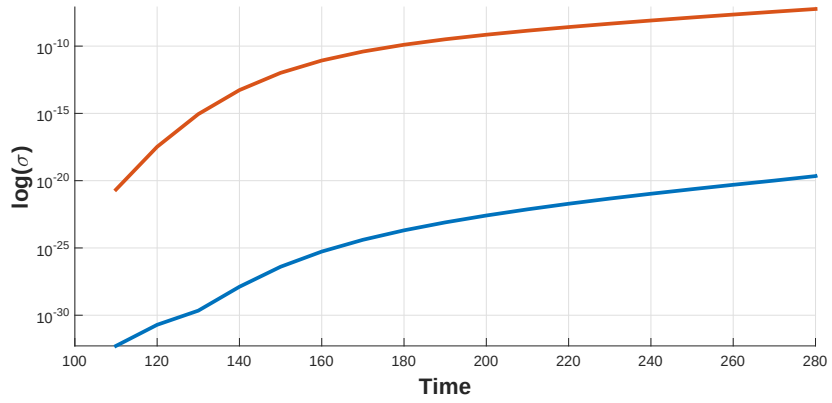

Figure 3.2: Comparison of the variance in logarithmic scale over time for the first method of absorption (red line) and the second one (blue line) discussed above. The conditions are the same of the Fig. 3.1.

Chapter 4

Results

Numerical results of a Bose-Einstein condensate evolution across different potentials in mean field approximation by the Gross-Pitaevskii equation are presented in this chapter.

The initial state is the wave function of the ground state prepared in the confining potential given by a one-dimensional harmonic trap $V_0 = \frac{1}{2}(x-x_0)^2$, which for the non-interacting problem is a Gaussian in the form $\psi(x,t=0) = A\exp(-x^2/2)$. A is the normalization constant, the interacting problem is analytically more complicated, but numerically it is calculated in the same way. Then the condensate is loaded instantaneously into our chosen engineered potential and left free to evolve through it.

In the first section we will see the evolution of a wave packet in free half space. Half space here means that the wave packet can only move towards the right because of the harmonic potential always present on the left. In the second section the evolution on the half tilted optical lattice will be presented. We will also show how the atom-atom interactions affect the evolution in these systems. Bloch oscillations are also presented, and how the interactions affect them. It is shown how the condensate behaves in very different ways when changing the parameters of the tilted optical lattice.

Our main observable for the study of the transport of ultracold atoms is the density current. In our units the current can be expressed as

$$j(x,t) = \frac{1}{2i}[\psi^*(x,t)\frac{\partial}{\partial x}\psi(x,t) - \psi(x,t)\frac{\partial}{\partial x}\psi^*(x,t)] \tag{4.1}$$

This observable strongly depends on the nature of the interaction (attractive or repulsive) and the strength of it, which is determined by the number of interacting atoms.

For a grid-step size of Δx, the time-dependent current at the grid point x_j is given by

$$j(x_j,t) = \frac{i}{2\Delta x}[\psi^*(x_j+\Delta x,t)\psi(x_j,t) - \psi^*(x_j,t)\psi(x_j+\Delta x,t)] \tag{4.2}$$

4.1 Evolution of a wave packet in free half space

The simplest case is shown in this section, in which we investigate the behaviour of a wave packet prepared in the ground state of an harmonic potential in the presence of the atom-atom interaction. For attractive interactions ($g < 0$) the initial wave packet will be more narrow, while for repulsive ones ($g > 0$) it will be wider. Then the wave is left free to evolve in the right half space as shown in Fig. 4.1.

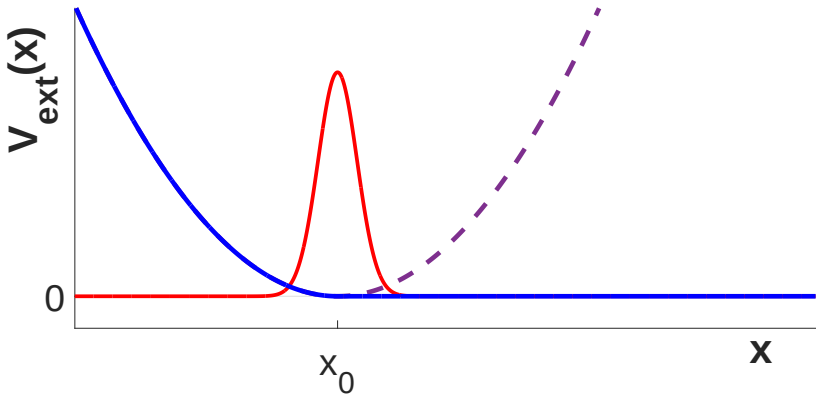

Figure 4.1: Sketch of the experiments we are proposing. The initial state (red solid lines) is prepared within an harmonic trap (blue lines for $x < x_0$ and viola dashed lines for $x > x_0$). The trap is released on the right part of x_0 to zero, which makes the initial wave packet move towards the right.

To understand how the interactions act we first plot the current density for different interaction strengths g measured at the point $x = 2x_0$, with $x_0 = 20.5$ (Fig. 4.1). It can be observed that the wave packet passes the point at which we measure the current with a characteristic maximum, whose precise position is determined by g. While for repulsive interactions the wave packet widens over time subject to diffusion, for attractive interactions, after a settling time, the wave packet keeps it's identity and moves as in classical regime as shown in Fig. 4.3.

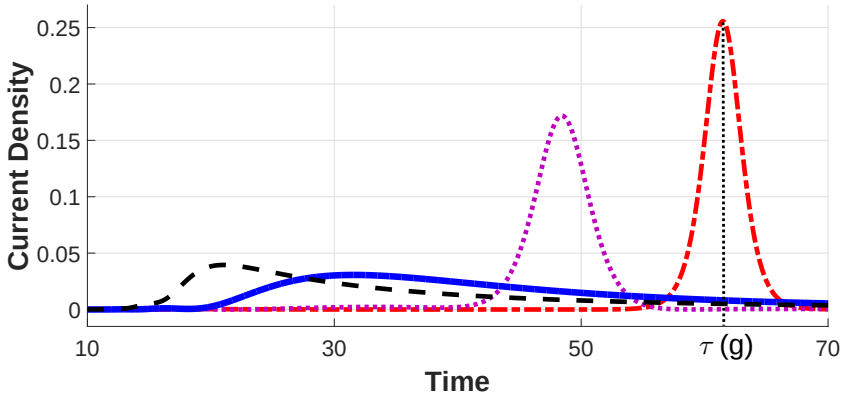

Figure 4.2: The particle current as a function of time at $x = 2x_0$ for the following values of interaction strength from left to right: $g = 2$ (black dashed line), $g = 0$ (blue solid line), $g = -1$ (viola dotted line), and $g = -2$ (red dot-dashed curve).We observe clear maxima of the currents, whose position on the time axis (denoted by τ) is determined by the sign and the strength of the non-linearity.

For repulsive interactions ($g > 0$), the wave packet tends to expand faster due to the additional repulsive potential term. For the attractive case ($g < 0$), the opposite happens and the wave packet tends to stabilize and the expansion is slowed down. In order to study the rates of these changes, we plot the dependence of the times τ when the maximum density is reached at $x = 2x_0$ in Fig. 4.4. While the qualitative behaviour of the enhanced expansion and the slowdown for positive and negative g, respectively, is clear (see also [50]), we have no analytic explanation so far for the scaling of $\tau(g)$ seen in Fig. 4.4.

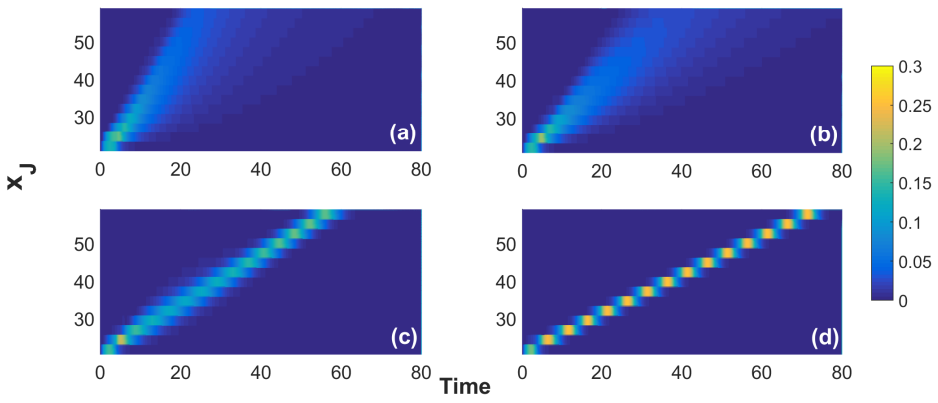

Figure 4.3: Three-dimensional comparison of the current in time calculated for different positions x_J and different interactions: (a) $g = 2$, (b) $g = 0$, (c) $g = -1$ (d) $g = -2$.

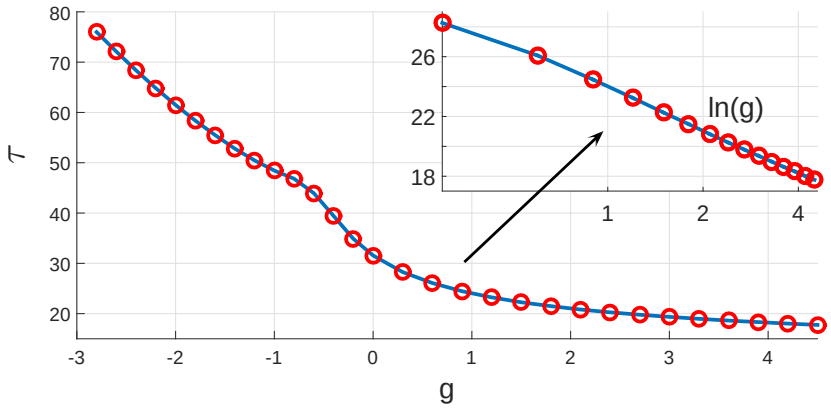

Figure 4.4: The times $\tau(g)$ of maximal current at position $x = 2x_0$ extracted from data sets such as shown in the previous figure. For positive non-linearities g, the scaling of the enhancement of the expansion seems logarithmic (see inset). For negative g, the expansion is slowed down a lot, which can be seen by the steep increase of the curve for decreasing $g < 0$.

4.2 Optical tilted lattice

The presence of an optical lattice slows down the expansion into it, while a constant negative tilt accelerates an initially localized wave packet towards the right. However, when both potential are present simultaneously, e.g. our setup shown in Fig. 4.5 , the situation is less clear. A tilted lattice problem defines the Wannier-Stark system, which was investigated with Bose condensates in great detail before, see section 2.5.

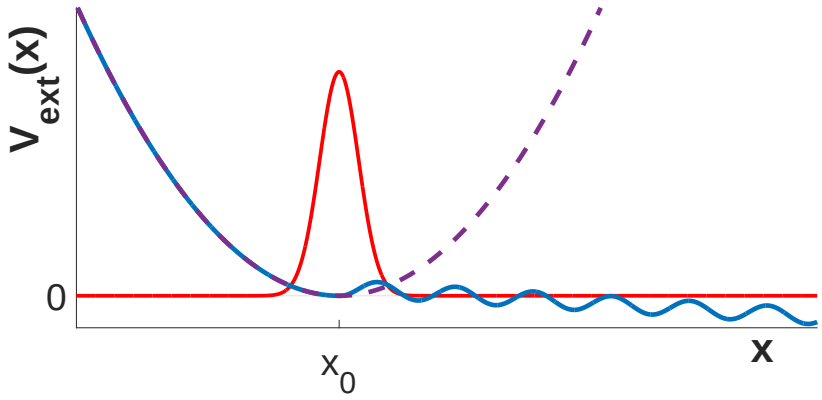

Figure 4.5: Schematic view of the potential we use, which is harmonic for $x < x_0$ and a Wannier-Stark ladder for $x > x_0$. We also show the starting wave function, which is the ground state of the potential (dashed line). From now on, the density current is calculated at the first relative maximum at the right of x_0, because, with this potential, most part of the wave will be localized only within a small range of space.

4.2.1 Oscillations of the current density

In this system, an initially localized wave packet remains localized but it oscillates with a characteristic Bloch frequency ω_B given by the constant level distance in the energy spectrum (arising from the constant spatial tilt). In our units, $\omega_B = F d_L$, where the d_L is the lattice spacing. This linear scaling of the oscillation frequency with the tilting force F is seen also in our expansion problem in the absence of interactions ($g = 0$). Because of the

presence of the harmonic confinement on the left, the proportionality factor is slightly lower than one, as seen in Fig. 4.6 (blue symbols connected by dotted line). Releasing also this left part of the trap, we instead observe the correct pre factor one, please see the red symbols in Fig. 4.6. The frequencies are extracted from the current oscillations to the right of (but close to) x_0 after a short initial transient, in which the wave packet adapts to the presence of the tilted lattice. It seems as if the potential left barrier reduces the effect of the Bloch oscillation.

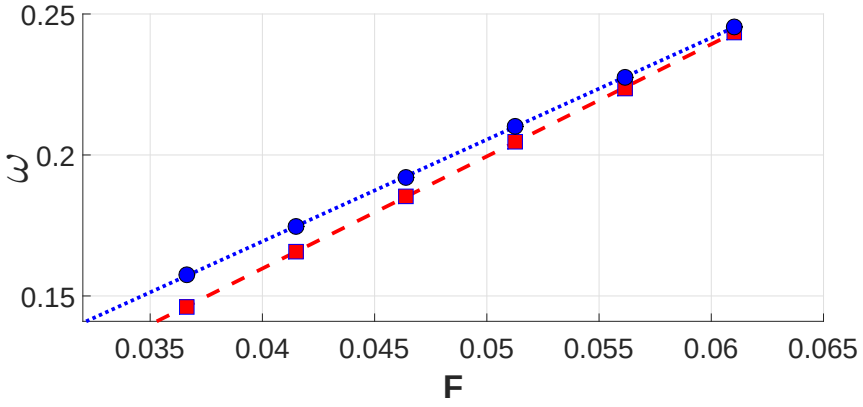

Figure 4.6: Oscillation frequency ω at $g = 0$ vs. the Stark (or gravity) force F for the case with left confinement (blue symbols connected by dotted line) and without it (red symbols connected by dashed line). In both cases, the scaling is linear as expected. The presence of the left part of the harmonic trap affects only the slope. The lattice parameters are $A = 1$ and $d_L = 4$.

More interesting is the oscillatory behaviour in the presence of interactions. We investigate again both cases of repulsive and attractive non-linearity. For now lets focus on the repulsive interactions. Our results are shown in Fig. 4.7. A repulsive interaction with $g > 0$ increases the oscillation frequencies. For not too large positive g, this increase is linear. For too large non-linearities a saturation is observed, see $g > 1$ in Fig. 4.7. Here the repulsion leads to a fast expansion which in turn decreases the density again. There our observed linear scaling of the oscillation frequency with the non-linear coupling parameter is theoretically predicted. Here we can

explain the initial linear increase in the oscillation frequency seen Fig. 4.7 by the local level shift induced by the non-linear potential term. This shift depends on the density in the lattice sites which is largest in the first well centred at x_0. This shift then leads to an effective increase of the difference ΔE of the two energy levels in the neighbouring wells, and consequently to a larger oscillation frequency. We may estimate

$$\Delta E = g \int_{1^{st}well} |\psi(x,t)|^2 dx - g \int_{2^{nd}well} |\psi(x,t)|^2 dx \approx g \int_{1^{st}well} |\psi(x,t)|^2 dx \tag{4.3}$$

Because of the oscillations, we take the time t of maximal density differences in the two wells for computing the above estimate. In principle, we can reduce the effect of the non-linear interactions by rescaling the tilting force from F to $F - F'$, where $F' \approx \Delta E/d_L$. This reduces the problem to the non-interacting one with the same Bloch-like oscillation frequency determined just by F alone. Corresponding numerical simulation for the current density are shown in Fig. 4.8 . Of course, our estimate is a bit too rough in order to be perfect for all times (in particular because of the time-dependence of the process). Yet, this possibility of controlling the dynamics of a Bose-Einstein condensate is quite interesting. We refer to similar situations where the effect of the interaction was approximately cancelled by applying appropriate external potentials in theory [51] and an actual experiment at Innsbruck [52].

We identified two different regimes, first a linear scaling and then a saturation. Here the theory developed by Kolovsky in [53] applies, and it predicts our observed linear scaling of the oscillation frequency with the non-linear coupling parameter. In Kolovsky's theory, a new period appears induced by the atomic interactions (in [53] shown using a many-body quantum model). In our regime of small and intermediate interactions therefore an additional period arises, beside the Bloch period, which is inversely proportional to the coupling strength.

The localization of the wave packet can be seen in the behaviour of the current, which oscillates around zero giving no average current over a

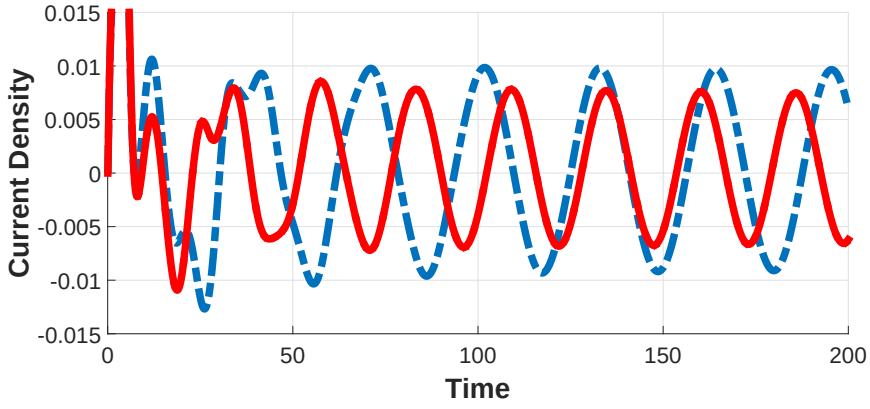

(a)

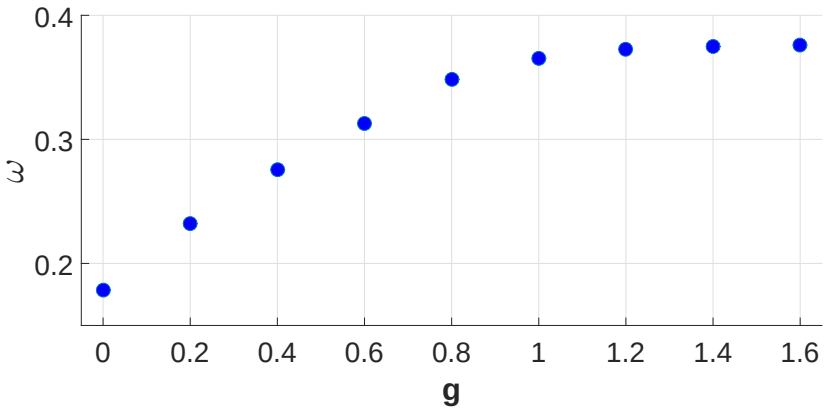

(b)

Figure 4.7: Comparison of the Bloch oscillations in the density current of a non-interacting packet (blue dashed line) and a repulsive one (red continuous line) (a). Dependence of the Bloch oscillation frequencies on the repulsive coupling constant ($g > 0$) (b). The first point on the left corresponds to the non-interactive case ($g = 0$). Every point was calculated with the same gravity force $F \approx 0.0427$, and same lattice parameters as in the previous figure.

period. Thus the choice of the point in which we measure the current must be near the first well, as shown in Fig. 4.9.

More complex is the case of attractive interactions with $g < 0$. Here for small $|g| < 1$, the Bloch-like oscillations are rather stable. For large $|g| > 1$, again the non-linearity potential dominates the dynamics, in the sense that the non-linear term is larger than the kinetic term. Here interaction-induced oscillations with a frequency $\omega \sim |g|$ occur. Here the density remains large

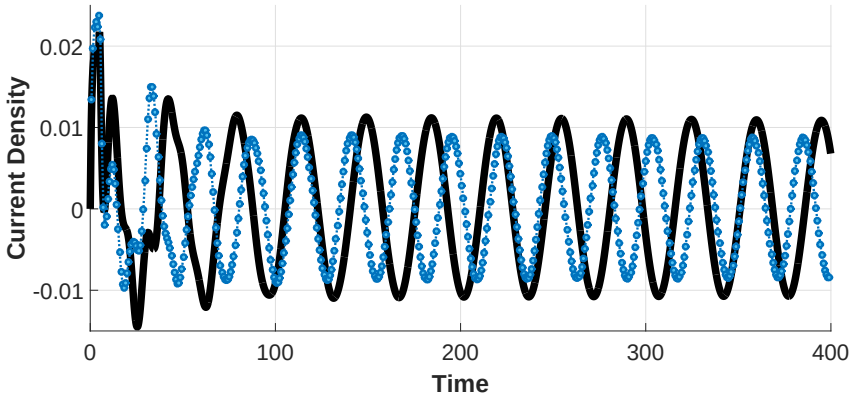

(a)

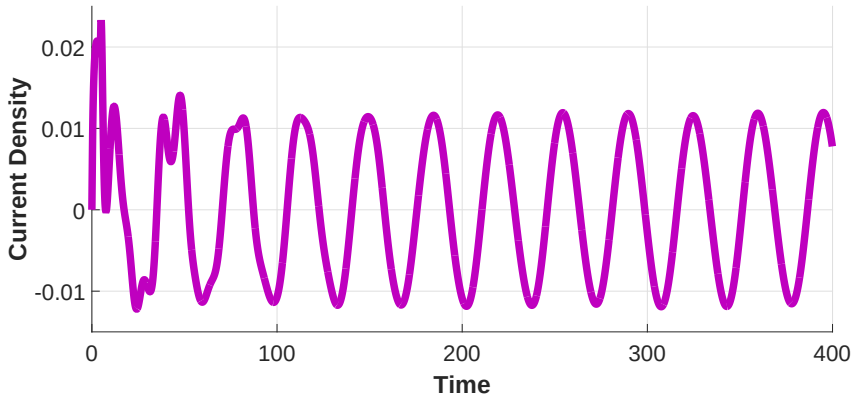

(b)

Figure 4.8: Temporal evolution of the current to the right but close to $x_0 = 20.5$ for the three cases: (a) $g = 0$; $F = 0.043$ (black solid line), $g = 0.2$; $F = 0.043$ (blue symbols), and (b) $g = 0.2$; $F = 0.043 - F' = 0.029$ (viola solid line). In (b) the non-linear shift of the local energy level (where the atomic density is large) is corrected by a reduction of the tilting force with $F' = 0.014$. We observe good agreement between the oscillation frequencies of the black (a) and the purple (b) curves. Lattices parameters as in previous figures.

also during the evolution because of the attractive forces.

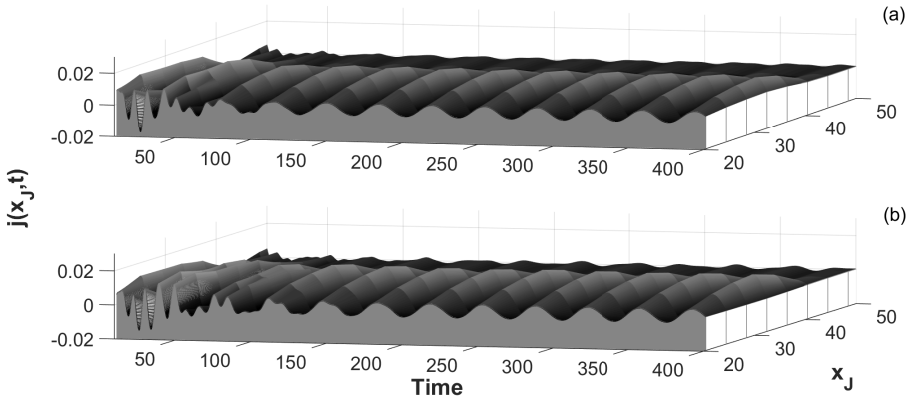

Figure 4.9: Three-dimensional comparison of the current in time calculated for different positions x_J: (a) for same parameters of the non-interacting system ($g = 0$) in Fig. 4.8(a) and (b) same parameters of Fig. 4.8(b).

4.2.2 No tilting force

To understand the compensation of the interaction to the force (shown in Fig. 4.8), we investigated the behaviour of the interacting condensate with no tilting force, which in the case of a non interacting condensate $g = 0$ would travel through the lattice indefinitely as shown in Fig. 4.11. Switching on the interactions the wave behave as if it is on a Wannier-Stark ladder with localized oscillations Fig. 4.11. The frequencies are not constant because the splitting of the energies' level, generated by the interactions, is not constant over time, but it's subject to oscillations.

4.3 Other results

The parameters of the optical lattice chosen in the previous section give a small amount of transport, for which the wave packet stays most localized in the first well. This behaviour is the reason why the repulsive interaction acts as an effective tilting force. To increase the transport due to the tunneling effect, the best option is to reduce the lattice spacing d_L which in the following will be fixed to $d_L = 3$. With this choice of parameters we cannot say that most of the wave packet is localized, but it is equally distributed

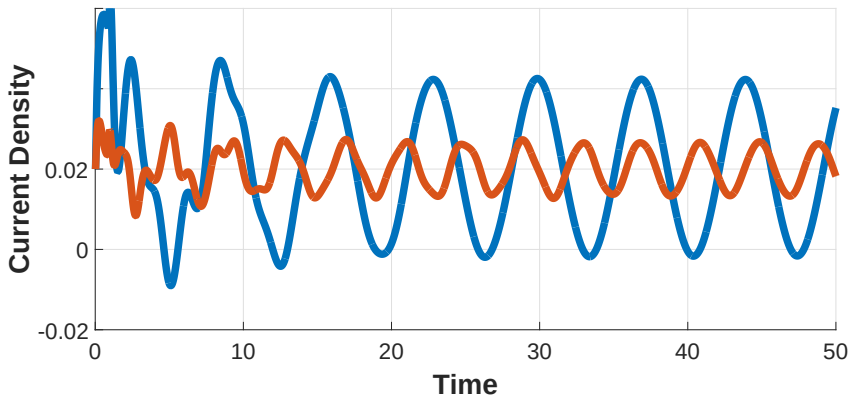

(a)

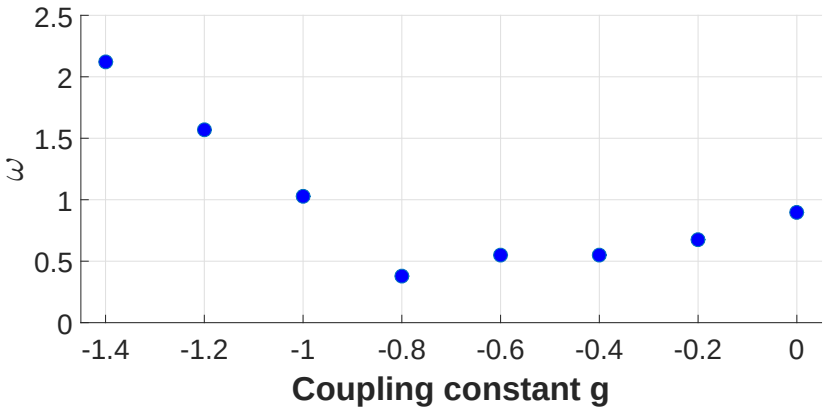

(b)

Figure 4.10: Comparison of the Bloch oscillations in density current of a non-interacting packet (blue dashed line) and attractive one (red continuous line) (a). Dependence of the Bloch oscillations' frequencies on the attractive coupling constant ($g < 0$) (b). The first point to the right correspond to a non-interactive coupling constant ($g = 0$). Every point calculated with the same gravity force $F \approx 0.0427$, and same lattice parameters as in the previous figures.

over more wells over time (see Fig 4.12).

With these chosen parameters, we can see a substantial transport though the potential, e.g. estimating the amount of the wave function that remains within a fixed range $0 < x < x_L$, which in our case is up to the tenth well ($x_L \simeq 68$). The observable can be written as $n(t) = \int_0^{x_L} |\psi(x,t)|^2 dx$ and will be shown in Fig. 4.13

The "permanence" of the wave function $n(t)$ in the firsts nine wells

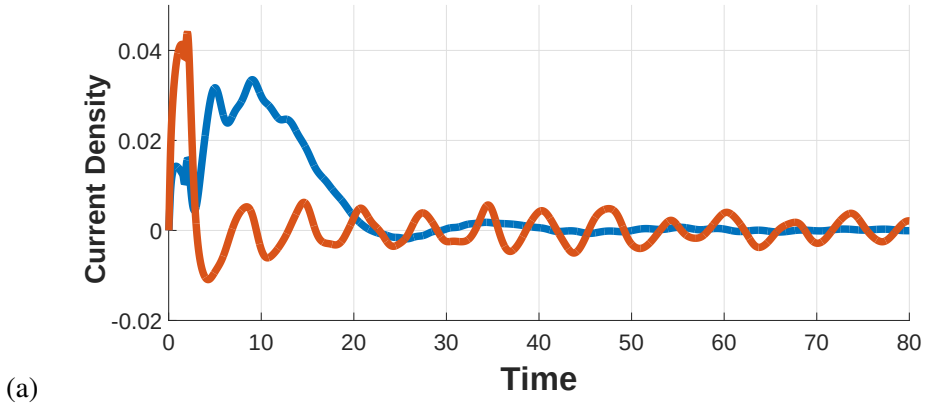

(a)

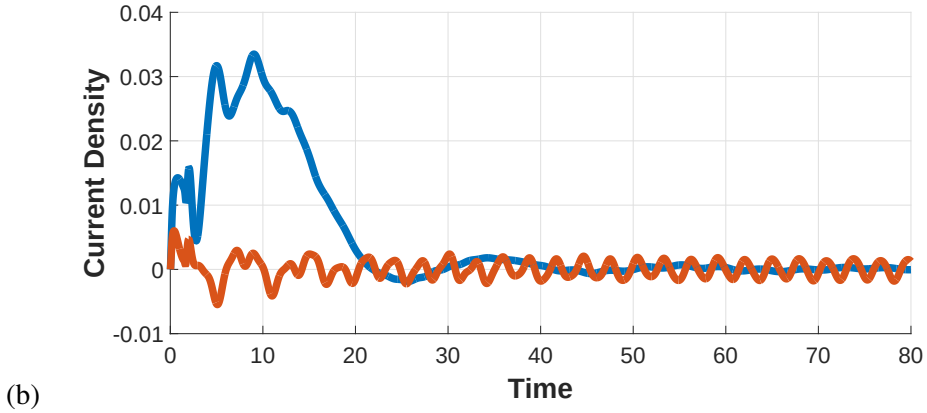

(b)

Figure 4.11: Comparison of the Density Currents of a non-interacting packet (blue line) and a repulsive one (red line) travelling through an optical lattice (a), and an attractive one (b). Here no gravity force is present.

shows an exponential decay, with an oscillating behaviour on top due to the Bloch oscillations.

The atom-atom interactions act now in a very different way respect the previous results (in Section 4.2.1). This time, due to the evenly distribution of the wave function and the maximum located in the minimum of the potential, the interaction raises (or reduces) each energy level, increasing (or decreasing) the tunneling effect. The attractive interaction raises up the energy levels, increasing the current density amplitude and speeding up the decay of the permanence in the firsts wells. Vice-versa the repulsive interaction increases the amplitude of the lattice, decreasing the current density

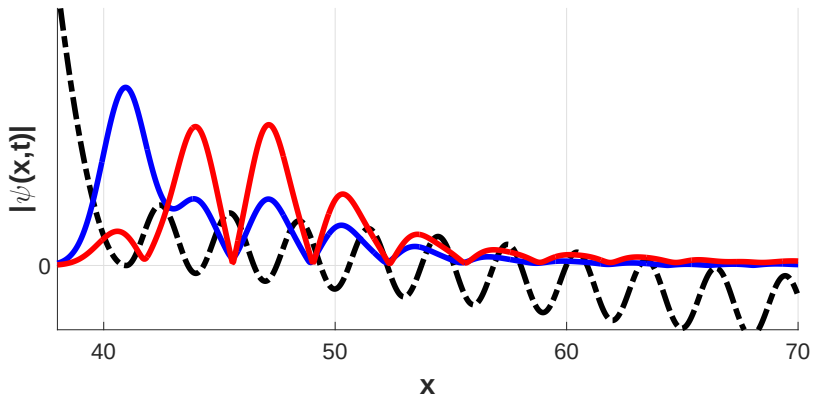

Figure 4.12: Evolved wave function $|\psi(x,t)|$ for different times $t = 1200$ (red line), and $t = 1400$ (blue line) over our engineered potential (dotted line)

amplitude and slowing down the decay of the permanence(see Fig. 4.14). Thus we can say that the interactions act as an effective contribution to the lattice amplitude after a small time in which the waves settles down to an evenly distributed state. After this time, the current density shows oscillations with frequencies $\omega \simeq F d_L$.

Here the continuous loss of wave make the shift of the energy levels dependent on time. Thus a constant perturbation on the lattice depth can be valid for short times or it must be made time dependent with the same decay over time as the permanence function of the non-interacting case.

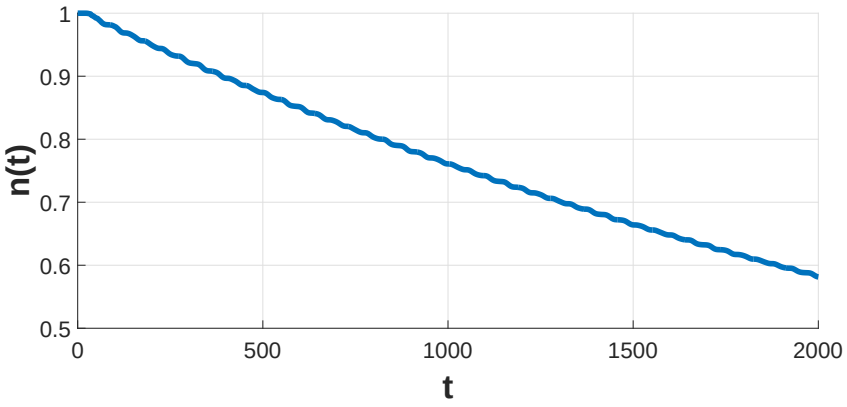

(a)

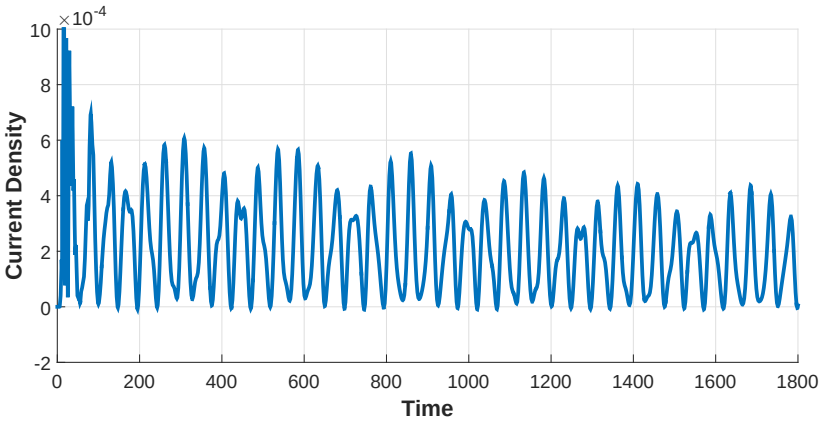

(b)

Figure 4.13: Temporal evolution of the permanence function (a) and current density (b) in the case of no interactions ($g = 0$), lattice spacing $d_L = 3$, lattice amplitude $A = 1$ and tilting force $F = 0.0407$. After a small initial time in which the wave-function settles from a Gaussian function to a Bloch state, it can be seen the characteristic Bloch oscillations. The current density is calculated at the point $x_J = x_L \simeq 68$.

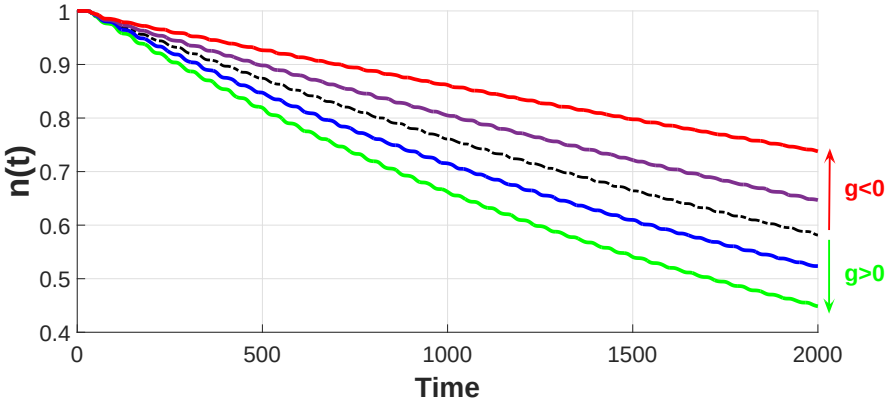

(a)

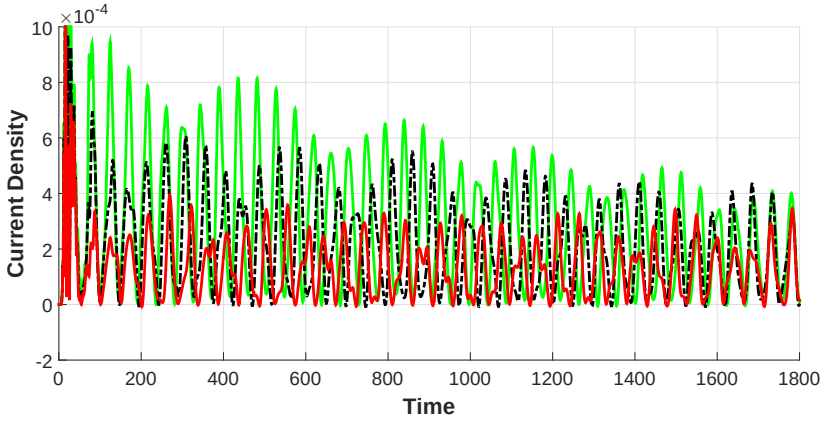

(b)

Figure 4.14: Temporal evolution of the permanence function (a) and the current density (b) with same potential parameters as in Fig. 4.13, for different interactions: non interacting atoms (black dotted line), repulsive with coupling constant $g = 0.15$ and $g = 0.05$ (green and blue lines respectively), attractive with $g = -0.15$ and $g = -0.05$ (red and purple lines respectively).

Chapter 5

Conclusions

Quantum transport in engineered potential provides a way to study the behaviour of ultracolds atoms in certain conditions and to provide proves of quantum theories developed in the solid state physics. In this thesis, we restricted to the simplified case of a one-dimensional setup for transport a Bose-Einstein condensate. We applied a mean-field approximation to include interaction-induced effects in the limit of weak and intermediate interaction strength. Our numerical results show how the transport can be controlled by adjusting the parameters of the engineered potential, in a specific but realistic setup. Our parameters include the depth and periodicity of an optical lattice,, the tilting force and the atom-atom interactions coupling constant. Moreover, our results show that for a sufficiently deep lattice and large periodicity, compared to the tilting force, the localization of the wave provides a simple way to make the non-linear term of the interactions approximated to an effective tilting force. Vice-versa decreasing the lattice periodicity, the non-linearity acts on each energy level, increasing (or decreasing) the tunneling.

5.1 Perspectives

Many open problems have remained which allow for further studies. During our work we tried to understand many problems which are not presented in the body of this thesis. Since the atom-atom interactions couple

the three orthogonal direction x, y, z, a three-dimensional system must be studied, thus we tried to reduce the problem of the transport of a Bose-Einstein condensate through a cigar-shaped three-dimensional trap, which requires a huge amount of calculation time, to a two-dimensional system, respecting the symmetries. The considered system is described by the radial variable $\rho \geq 0$ and the longitudinal variable x. The potential $V(\vec{r})$ is considered radially symmetric, so in principle this system can be described by the two-dimensional Gross-Pitaevskii equation in cylindrical coordinates.

$$\begin{aligned} i\frac{\partial}{\partial t}\psi(x,\rho,t) &= H(x,\rho,t)\psi(x,\rho,t) \\ H(x,\rho,t) &= -\frac{1}{2}\left(\frac{\partial^2}{\partial x^2}+\frac{\partial^2}{\partial \rho^2}+\frac{\partial^2}{\rho\partial\rho}\right)+V_{ext}(x,\rho)+g_{3D}|\psi(x,\rho,t)|^2 \end{aligned} \tag{5.1}$$

The first partial derivative in ρ causes problems in the integration scheme given in Eq. 3.6, because the expansion over a grid of the Hamiltonian becomes asymmetric, which makes the discrete evolution operator non unitary. This causes a non constant normalization, which especially in our case, where the wave is absorbed by the boundary, is important to remain constant.

Our partial solution of the problem consists on finding the solution for $\psi(x,\rho) = \frac{\chi(\rho)}{\rho^{1/2}}\phi(x)$, which removes the problem of the first derivative in the kinetic energy of the radial part.

$$T_\rho\psi(x,\rho) = -\frac{1}{2}\frac{1}{\rho}\frac{\partial}{\partial\rho}\rho\frac{\partial}{\partial\rho}\psi(x,\rho) \tag{5.2}$$

$$T_\rho\chi(\rho) = -\frac{1}{2}\left(\frac{\partial^2}{\partial\rho^2}+\frac{1}{4\rho^2}\right)\chi(\rho) \tag{5.3}$$

Now the finite element method gives a symmetric Hamiltonian matrix, thus it doesn't give any problem regarding the conservation of the wave function's normalization, but another problem arises. Here the term $\frac{1}{4\rho^2}$ diverges in $\rho = 0$, which is where the wave function $\psi(x,\rho)$ has it's maximum, so it cannot be simply avoided. The simplest way to avoid this issue, is to act manually on the first element of the Hamiltonian matrix.

Bibliography

[1] J. P. Brantut, J. Meineke, D. Stadler, S. Krinner, and T. Esslinger, Science **337** (2012) 1069;

[2] S. Krinner, D. Stadler, D. Husmann, J. P. Brantut, and T. Esslinger, Nature **517** (2015) 64;

[3] S. Eckel, J. G. Lee, F. Jendrzejewski, N. Murray, C. W. Clark, C. J. Lobb,W. D. Phillips, M. Edwards, and G. K. Campbell, Nature **506** (2014) 200

[4] R. Labouvie, B. Santra, S. Heun, S. Wimberger, and H. Ott, Phys. Rev. Lett. **115** (2015) 050601

[5] C. Waschke, H. G. Roskos, R. Schwedler, K. Leo, H. Kurz, and K. Köhler, Phys. Rev. Lett. **70**, 3319 (1993).

[6] M. Ben Dahan, E. Peik, J. Reichel, Y. Castin, and C. Salomon, Phys. Rev. Lett. **76**, 4508 (1996).

[7] B. Anderson and M. Kasevich, Science **282**, 1686 (1998).

[8] O. Morsch, M. Oberthaler, Rev. Mod. Phys. **78**, 179 (2006).

[9] R. P. Feynman, Int. J. Theor. Phys. **21**, 467 (1982).

[10] O. Morsch, J. H. Muller, M. Cristiani, D. Ciampini, and E. Arimondo, Phys. Rev. Lett. **87** 140402 (2001).

[11] C. J. Pethick and H. Smith, Bose-Einstein Condensation in Dilute Gases (Cambridge University Press, Cambridge, 2002); L. Pitaevskii

and S. Stringari, Bose-Einstein Condensation (Oxford University Press, Oxford, 2003).

[12] S. Wimberger, R. Mannella, O. Morsch, E. Arimondo, A. R. Kolovsky, and A. Buchleitner, Phys. Rev. A **72**, 063610 (2005).

[13] C. Sias, A. Zenesini, H. Lignier, S. Wimberger, D. Ciampini, O. Morsch, and E. Arimondo, Phys. Rev. Lett **98**, 120403 (2007).

[14] A. Zenesini, C. Sias, H. Lignier, Y. Singh, D. Ciampini, O. Morsch, R. Mannella, E. Arimondo, A. Tomadin and S. Wimberger, New J. Phys. **10**, 053038 (2008).

[15] M. Holthaus, J. Opt. B: Quantum Semiclassical Opt. **2**, 589 (2000).

[16] S. N. Bose, Z. Phys. **26**, 178 (1924).

[17] A. Einstein, Sitzungsberichte der Preussichen Akademie der Wissenchaften, Physikalish-mathematische Klasse p.261 (1924); p. 3 (1925).

[18] H. Feshbach, Ann. Phys. **5**, 357 (1958)

[19] P. Lebedev, Ann. Phys. **32**, 411 (1910); O. Frish, Z. Phys. **88**, 42 (1933).

[20] A. F. Bernhardt, D. E. Duerre, J.R. Simpson, and L. L. Wood, Appl. Phys. Lett. **25**, 617 (1974); E. Arimondo, H. Lew, and T. Oka, Phys. Rev. Lett. **43**, 753 (1979).

[21] J. E. Bjorkholm, R. E. Freeman, A. Ashkin, and D. B. Pearson, Phys. Rev. Lett. **41**, 1961 (1978); Steven Chu, J. E. Bjorkholm, A. Ashkin, and A. Cable, Phys. Rev. Lett. **57**, 314 (1986).

[22] P. C. M. Planken, M. C. Nuss, I. Brener, K. W. Gossen, M. S. C. Luo, S. Lien Chuang and Loren Pfeiffer, Phys. Rev. Lett. **69**, 3800 (1992).

[23] E. E. Mendez, G. Bastard, Phys. Today **46**, 34 (1993).

[24] M. Greiner, O. Mandel, T. Esslinger, T. W. Hansch, and I. Bloch, Nature **415**, 39 (2002).

[25] I. Bloch, Nature, **1**, 23 (2005).

[26] C. Cohen-Tannoudji, J. Dupont-Roc, G. Grynberg, Atom-Photon Interactions, Wiley and Sons, New York, **206**, 209 (1992).

[27] R. Grimm, M. Weidemuller, and Y. B. Ovchinnikov, Advances in Atomic, Molecular and Optic Physics, **42**, 95, (2000).

[28] F. Bloch, Zeitschrift fur Physik, **52**, 555 (1928).

[29] C. Zener, Proc. Roy. Soc. London Ser., **145**, 523 (1934).

[30] L. Esaki, R. Tsu, IBM J. of Research and Development, **14**, 61 (1970).

[31] G. H. Wannier, Phys. Rev. **117**, 432 (1960); Rev. Mod. Phys. **34**, 645 (1962); Phys. Rev. **181**, 1364 (1969).

[32] J. E. Avron, J. Zak, A. Grossmann, and L. Gunther, J. Math. Phys. **18**, 918 (1977).

[33] J. B. Krieger and G. J. Iafrate, Phys. Rev. B **33**, 5494 (1986); ibid., **38**, 6324 (1988).

[34] G. Nenciu, Rev. Mod. Phys. **63**, 91 (1991).

[35] M. Luban, A. Bouchard, Phys. Rev. B **47**, 6815 (1993).

[36] P. Voisin, J. Bleuse, C. Bouche, S. Gaillard, C. Alibert, and A. Regreny, Phys. Rev. Lett. **61**, 1639 (1988); E. E. Mendez, F. Agull-Rueda, and J. M. Hong, Phys. Rev. Lett. **60**, 2426 (1988).

[37] M. Gluck, A. R. Kolovsky, and H. J. Korsch, Phys. Rev. Lett. **83**, 891 (1999).

[38] N. Moiseyev and H. J. Korsch, Phys. Rev. A **41**, 498 (1990); M. Gluck, A. R. Kolovsky, H. J. Korsch, and N. Moiseyev, Eur. Phys. J. D **4**, 239 (1998).

[39] S. Glutsch and F. Bechstedt, Phys. Rev. B **60**, 16 584 (1999).

[40] M. Gluck, A. R. Kolovsky, and H. J. Korsch, Phys. Rev. Lett. **83**, 891 (1999).

[41] B. Rosam, D. Meinhold, F. Loser, V. G. Lyssenko, S. Glutsch, F. Bechstedt, F. Rossi, K. Köhler, and K. Leo, Phys. Rev. Lett. **86**, 1307 (2001).

[42] H. Schneider, H. T. Grahn, K. v. Klitzing, and K. Ploog, Phys. Rev. Lett. **65**, 2720 (1990).

[43] R. Till, H. Kummel, A. Philipp, G. B¨ohm, and G. Weimann, Superlattices Microstruct. **24**, 227 (1998).

[44] W. H. Press, S. A. Teukolsky, W. T. Vetterling und B. P. Flannery, Numerical Recipes, Cambridge University Press, Cambridge (2002).

[45] W. A. Ames, Numerical Methods for Partial Differential Equation, Academic Press, New York (1977).

[46] M. L. Chiofalo, S. Succi, und M. P. Tosi, Phys. Rev. E **62**, 7438 (2000).

[47] J. Lysemer and R. L. Klihlemeyer, J. Eng. Mech. Div. Proc. Amer. Sot. Civil Eng. **95** (1969), 859.

[48] R. Clayton and B. Enquist, Bull. Seismol. Sot. Amer. **67** (6) (1977), 1529.

[49] A. C. Reynolds, Geophysics **43** (6) (1978), 1099.

[50] M. J. Holland and J. Cooper, Phys. Rev. A 53 (1996) R1954; M. J. Holland, D. S. Jin, M. L. Chiofalo, and J. Cooper, Phys. Rev. Lett. **78** (1997) 3801; S. K. Adhikari, J. Phys. B: At. Mol. Opt. Phys. **36** (2003) 3951.

[51] S. Micciche, A. Buchleitner, F. Lillo, R. Mantegna, T. Paul, and S. Wimberger, New J. Phys. **15** (2013) 033033

[52] M. Gustavsson, E. Haller, M. J. Mark, J. G. Danzl, R. Hart, A. J. Daley, H.-C. Nägerl, New J. Phys. **12** (2010) 065029

[53] A. R. Kolovsky, Phys. Rev. Lett. **90** (2003) 213002.

Acknowledgement

Ringraziamenti